Numerical Investigation of Multistaged Tesla Valves

S. M. Thompson[1]
Department of Mechanical Engineering &
Center for Advanced Vehicular Systems,
Mississippi State University,
Mississippi State, MS 39762
e-mail: thompson@me.msstate.edu

B. J. Paudel
Department of Mechanical Engineering &
Center for Advanced Vehicular Systems,
Mississippi State University,
Mississippi State, MS 39762

T. Jamal
Department of Mechanical Engineering &
Center for Advanced Vehicular Systems,
Mississippi State University,
Mississippi State, MS 39762

D. K. Walters
Department of Mechanical Engineering &
Center for Advanced Vehicular Systems,
Mississippi State University,
Mississippi State, MS 39762

The Tesla valve is a passive-type check valve used for flow control in micro- or minichannel systems for a variety of applications. Although the design and effectiveness of a singular Tesla valve is somewhat well understood, the effects of using multiple, identically shaped Tesla valves in series—forming a multistaged Tesla valve (MSTV)—have not been well documented in the open literature. Therefore, using high-performance computing (HPC) and three-dimensional (3D) computational fluid dynamics (CFD), the effectiveness of an MSTV using Tesla valves with preoptimized designs was quantified in terms of diodicity for laminar flow conditions. The number of Tesla valves/stages (up to 20), valve-to-valve distance (up to 3.375 hydraulic diameters), and Reynolds number (up to 200) was varied to determine their effect on MSTV diodicity. Results clearly indicate that the MSTV provides for a significantly higher diodicity than a single Tesla valve and that this difference increases with Reynolds number. Minimizing the distance between adjacent Tesla valves can significantly increase the MSTV diodicity, however, for very low Reynolds number ($Re < 50$), the MSTV diodicity is almost independent of valve-to-valve distance and number of valves used. In general, more Tesla valves are required to maximize the MSTV diodicity as the Reynolds number increases. Using data-fitting procedures, a correlation for predicting the MSTV diodicity was developed and shown to be in a power-law form. It is further concluded that 3D CFD more accurately simulates the flow within the Tesla valve over a wider range of Reynolds numbers than 2D simulations that are more commonly reported in the literature. This is supported by demonstrating secondary flow patterns in the Tesla valve outlet that become stronger as Reynolds number increases. Plots of the pressure and velocity fields in various MSTVs are provided to fully document the complex physics of the flow field. [DOI: 10.1115/1.4026620]

Keywords: Tesla valve, no-moving-parts valve, diodicity, multistage check valve, check valve, microfluidics, flow control, CFD

Introduction

Passive flow control in mini/microchannels can be accomplished by integrating no-moving-parts check valves (NMPVs) [1–5]. Due to their unique structural design, NMPVs possess a direction-dependent pressure drop, resulting in the promotion of one flow direction over another. Depending on flow direction, minor pressure losses may be higher (reverse flow) or lower (forward flow), effectively creating a fluidic diode. NMPVs are easily scalable and manufacturable and, unlike micropumps with moving parts, can be used with colloidal suspensions with no detriment. For these reasons, NMPVs have been used for pumping/mixing in applications such as: microelectromechanical systems (MEMS), biotechnological devices, and analytical chemistry [1]. Three examples of NMPVs are the diffuser (a.k.a. sudden-expansion) valve [2–4], heart-shaped valve [5], and Tesla valve [1,6–15].

The Tesla valve, first introduced by N. Tesla as a "valvular conduit" circa 1920 [6], functions by passively promoting one flow direction over another via its unique dual-vein, arclike design, as shown in Fig. 1. During reverse flow through a Tesla valve, minor pressure losses are primarily due to bifurcation (flow splitting), sudden expansion, and jet impingement. The effectiveness of a Tesla valve (and other NMPVs) is typically measured via diodicity Di, which is the ratio of the pressure difference across the valve in the reverse and forward directions for a specific flow rate, i.e.

$$Di = \left.\frac{\Delta P_r}{\Delta P_f}\right|_{\dot{V}} \tag{1}$$

A greater-than-unity diodicity indicates flow promotion in the forward direction. For microscale Tesla valves, the diodicity is typically between 1 and 2 [7]. However, for macroscale Tesla valves ($D_H \sim 10$ cm), the diodicity can achieve values on the order of four due to dynamic flow effects (high Re) becoming more significant [8].

Forster et al. experimentally determined the effectiveness (i.e., diodicity) of a diffuser valve and (separately) Tesla valves in line with a piezoactuated pump [1]. The fabricated Tesla valve was termed the T45-R due to it possessing a 45 deg vein angle, similar to Fig. 1. Two T45-R valves were fabricated onto a silicon wafer and each possessed a channel width and depth of 114 μm and 60 μm, respectively. For low Reynolds number flow ($Re < 300$), it was found that the T45-R Tesla valve's diodicity increased linearly with flow rate. At a flow rate of 500 μL/min ($Re \cong 180$), the diodicity was measured to be approximately 1.14. The feasibility of using Tesla valves for microfluidics was clearly demonstrated and it was shown that Tesla valves possess a higher diodicity than their diffuser check valve counterparts.

Truong and Nguyen conducted a numerical study on a single Tesla valve in order to determine its optimal design features for various flow rates ($Re < 1000$) [9]. Two-dimensional (2D), steady-state numerical simulations were conducted using ANSYS FLOTRAN 6.0. The optimization was based on the Forster et al. T45-R Tesla valve as a reference design. The numerically predicted diodicity [9] of the T45-R at various flow rates ($100 < Re < 600$) was validated to be within 10% (overpredicting) of the Forster et al. experimental results [1]. Multiple correlations were provided for determining the optimal Tesla valve geometry for low Reynolds number.

Bardell investigated both experimentally and numerically, in great detail, the diodicity associated with various Tesla valve designs for low Reynolds numbers [7]. Numerical data were

[1]Corresponding author.

Contributed by the Fluids Engineering Division of ASME for publication in the JOURNAL OF FLUIDS ENGINEERING. Manuscript received September 30, 2013; final manuscript received January 27, 2014; published online May 12, 2014. Assoc. Editor: Daniel Maynes.

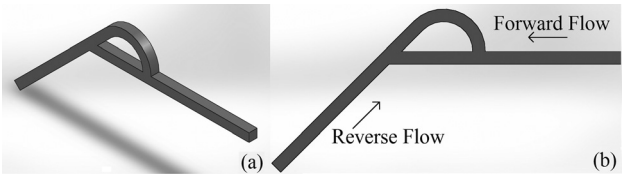

Fig. 1 (*a*) Tesla valve and (*b*) forward and reverse flow directions

obtained from a 2D simulation with the solver ANSYS CFX 4.2 and were validated with self-collected experimental results. Various case studies were undertaken to demonstrate the optimization routine for a Tesla valve. The diodicity mechanism of the Tesla valve at low Reynolds number was found to depend primarily on viscous forces, laminar jets (with varying location and magnitude), high energy-dissipation regions, and recirculation regions [7].

Zhang et al. performed a three-dimensional (3D) numerical simulation on a T45-R Tesla valve in order to determine optimal valve aspect ratio and other design features [10]. Numerical simulations were performed using ANSYS FLUENT® 6.2 for Reynolds number as high as 2000. Details regarding the laminar/turbulence solving methods were not clearly provided nor were verifications of the utilized solution method. It was found that the diodicity increases with flow rate and that for low Reynolds numbers ($\mathrm{Re} < 500$), a unity channel aspect ratio provides for maximal diodicity. For higher Reynolds numbers a Tesla valve channel with higher aspect ratio is desirable.

Gamboa et al. optimized the Tesla valve shape for application with piezoactuated plenums [11]. Six nondimensional, independent geometric design parameters were used in the optimization procedure, which utilized 2D numerical simulations. In general, the optimized Tesla valve, here deemed the Gamboa, Morris, and Forster (GMF) Tesla valve, provided a 25% higher diodicity compared to the standard T45-R Tesla valve design with no detriment to forward flow resistance. Their experimental results demonstrated that the diodicity predicted by 2D CFD was significantly higher than the experimentally determined diodicity.

Thompson et al. [12] integrated capillary/miniscale ($\sim$1 mm) Tesla valves into a flat-plate oscillating heat pipe (FP-OHP) for rectifying its highly oscillatory flow pattern in order to enhance its heat transfer capability. Using neutron radiography, the internal flow was visualized and, via image analysis techniques, the fluid motion was tracked. It was determined that the Tesla valves rectified the internal liquid motion and successfully promoted a net "circulatory flow," thus increasing heat transfer. The overall diodicity was found to increase as the internal liquid speeds increased with heat input [12].

A multistaged Tesla valve (MSTV) is the in-series configuration of multiple, identically shaped Tesla valves (a.k.a. stages). The motive for the MSTV design is based on the intuition that using multiple Tesla valves increases the reverse flow resistance and, thus, amplifies the fluidic diode effect [6,13–15]. The MSTV was first introduced, in concept, as the valvular conduit circa 1920 by N. Tesla, specifically for gas flows at the macroscale [6]. In 1993, Reed extended Tesla's valvular conduit [6] and produced a patent for an MSTV, termed a "fluidic rectifier," designed for high Reynolds number flow of gases [13]. For a MSTV with six valves, the diodicity was reported to be as high as 12. In 1999, Afromowitz et al. produced a patent for a MSTV designed for microfluidic applications [14]. Various design schemes for the MSTV were provided and a plenum-structured, piezoactuated pump was integrated into the system. Note that the valvular conduit concept was actually first integrated at the microscale for passive flow control of liquids by Forster et al. in 1995 [1].

Tesla valves within an MSTV may be connected in various configurations. An important example is, for reverse flow, the relative positioning of the downstream Tesla valve's entrance to its upstream neighbor. In order to quantify this relative positioning, an intervalve (or stage) angle θ is introduced, which is the angle between adjacent Tesla valve entrances. For illustration, as shown in Fig. 2(*a*), Reed's MSTV [13] has an intervalve angle equivalent to $\theta = \gamma + \alpha$. Since Reed's design provides for an MSTV with $\theta < 90$ deg, the intervalve flow is straighter and this MSTV may be referred to as "low-angled." In contrast, a "high-angled" MSTV provides for $\theta \geq 90$ deg. As an example, a high-angled MSTV with $\theta = 90$ deg is shown in Fig. 2(*b*) [14].

Mohammadzadeh et al. [15] used 2D CFD to numerically investigate the effect of the number of Tesla valves and Reynolds number on the diodicity of a high-angled MSTV and directly compared the results to that of a diffuser-type NMPV. The number of Tesla valves was varied from one to four and Reynolds number was varied up to 200. It was found that as the number of Tesla valves increased, the MSTV diodicity increased for Reynolds number greater than 50. It was suggested that the two-stage MSTV is optimal in order to decrease overall pressure drop and for ease of manufacture. The diodicity enhancement after implementing the second stage was found to be less significant. It was demonstrated that the high-angled MSTV is superior to the diffuser-type NMPV for relatively higher Reynolds numbers (i.e., $\mathrm{Re} > 200$), but inferior at lower Reynolds numbers. The four-staged MSTV provided for a diodicity of 2.6 at a Reynolds number of 200.

Since MSTVs can provide for enhanced diodicity, their application is of immediate interest for many micro/minifluidic systems. In terms of future application, low-angled MSTVs may provide for a lower overall diodicity compared to high-angled MSTVs [15], but their main appeal is their lower forward flow pressure loss, which is desirable for rectification of pulsating flows and active pump integration. Therefore, this study focuses on the numerical investigation of a low-angled MSTV consisting of individual GMF Tesla valves (preoptimized valves). The effect of the number of Tesla valves and Reynolds number on the MSTV diodicity is investigated for laminar flow conditions. The accuracy of 3D CFD in simulating Tesla valve flow is also discussed in detail. Various contours of static pressure and velocity are included to characterize the flow behavior within the MSTV. This numerical investigation is unique in that high performance computing was utilized, allowing for the use of highly refined meshes and the study of very long MSTVs (up to 20 stages). Unlike Ref. [15], the valve-to-valve distance is investigated and the number of stages is varied to be much greater than four stages. The investigated MSTVs, unlike Ref. [15], consist of preoptimized Tesla valves, and the low-angled design allows for broader range of applications.

Problem Setup

Using 3D CFD, the effect of Reynolds number, number of Tesla valve stages, and valve-to-valve distance were investigated to characterize their effect on the diodicity of a multistaged Tesla valve (MSTV) with low-angled configuration. First, in order to validate the CFD meshing scheme and procedure, the flow within a single T45-R Tesla valve [1,9], as shown in Fig. 1, was investigated. The T45-R Tesla valve had a square cross section with

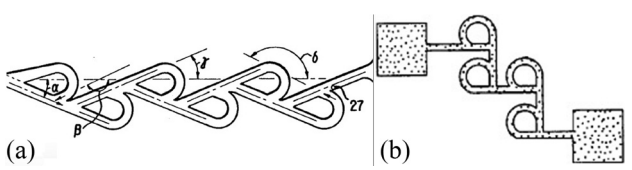

Fig. 2 Fluidic rectifier/multistaged Tesla valve (MSTV) with (*a*) low-angled configuration [13] and (*b*) high-angled configuration [14]

width of 100 μm. The Reynolds number at the inlet, $\mathrm{Re_i}$, was defined as

$$\mathrm{Re_i} = \frac{\rho u_i D_H}{\mu} \tag{2}$$

where u_i is the uniform inlet velocity (with respect to forward or reverse flow). The diodicity, found via Eq. (1), utilized the absolute, mass-averaged static pressure difference between points (a) and (b) as shown in Fig. 3. These points also correspond to the original entrance and exit lengths (0.6 mm) utilized by Truong and Nguyen [9]. Note that for the current investigation, the entrance and exit lengths were extended by a distance of 15 mm (on either side) in order to establish fully developed flow conditions and to resolve any potential issues related to reverse flow at the pressure outlet boundary condition.

An unstructured, three-dimensional hexahedral grid was built using ANSYS GAMBIT, with a total of 400,000 cells, based on the results of a mesh resolution study (to be described). Because the flow was at low Reynolds number, viscous effects are not strongly confined to the near-wall region and it was determined that a stretched near-wall prism layer was not necessary in order to accurately resolve near-wall velocity gradients. The characteristic mesh edge spacing was uniform throughout the mesh with a value of 0.05 D_H.

The boundary conditions included velocity inlet, pressure outlet, and no-slip (wall) conditions. Location of velocity inlet and pressure outlet boundary conditions depended on whether forward or reverse flow was being simulated. For each Reynolds number, the component of velocity was changed accordingly while the fluid was maintained as liquid water at a temperature of 293 K.

Numerical solutions were obtained for the single-phase, incompressible Navier–Stokes equations, with constant fluid properties

$$\frac{\partial u_i}{\partial t} + \frac{\partial (u_i u_j)}{\partial x_j} = -\frac{1}{\rho}\frac{\partial P}{\partial x_i} + \nu \frac{\partial^2 u_i}{\partial x_j \partial x_j} \tag{3a}$$

$$\frac{\partial u_j}{\partial x_j} = 0 \tag{3b}$$

Simulations were carried out using a pressure-based, finite-volume, double precision 3D commercial flow solver (ANSYS FLUENT® Version 14). The Semi-Implicit Method for Pressure Linked Equations (SIMPLE) algorithm [16] was used for the pressure-velocity coupling. A colocated variable arrangement was used with momentum weighted interpolation for computation of the pressure and mass flux at cell faces [17]. The convective terms were discretized using a second-order upwind (linear reconstruction) scheme with slope limiting [18] and spatial gradients computed using a cell-based least squares algorithm. Diffusion terms were discretized using second-order central differencing. Default underrelaxation factors were used. Steady-state simulations were conducted until the root mean square (rms) values of the continuity and velocity residuals were reduced to at least 1E-6 of their initial values. For unsteady simulations, a second-order, three-point backward difference scheme was used for discretization of the local time derivative, and the rms values of the residuals were reduced at least three orders of magnitude during each time step.

It was determined that complete laminar conditions would exist throughout the entire Tesla valve structure—especially near the valve exit where larger channel widths and jet impingement exist—only for Re $\lesssim$ 300. Larger Reynolds numbers resulted in local transitional flows within the valve structure, which manifested as unsteady instabilities in the computed flow field, even when the simulations were run using a steady-state algorithm. When these instabilities occurred, unsteady simulations were conducted, using global time stepping and a maximum convective Courant–Friedrichs–Lewy (CFL) number approximately equal to one. For these unsteady simulations the flow remained unstable, and it was determined that the flow had entered the early stages of the transitional regime for Re $\gtrsim$ 300.

A mesh-independence study was performed for the primary quantity of interest (diodicity) at the highest Reynolds number investigated (Re = 300) using both 2D and 3D flow simulations. The 3D results are shown in Fig. 4, in which the diodicity is plotted versus mesh resolution (number of cells). It was found that the diodicity changed less than 0.2% for the entire cell range investigated. Approximately 400,000 total cells were deemed sufficient for each Tesla valve (excluding extended entrance/exit lengths) for ensuring mesh-independent solutions and this was adhered to for the entire investigation. For the 2D simulations, it was separately found that a mesh-independent solution existed for approximately 40,000 cells.

The employed numerical scheme was further validated by comparing the 3D and 2D diodicity of the T45-R Tesla valve with the 2D numerical results of Truong and Nguyen [9] and the experimental results of Forster et al. [1] for low Reynolds numbers. These results are shown in Fig. 5. It may be seen that the current 3D T45-R diodicity approaches the Forster et al. experimental data with (1) a different trend and (2) significantly less error relative to the 2D CFD diodicity. This different trend can be partially attributed to 3D effects, e.g., secondary flows, not being fully resolved using 2D models. The current 2D CFD diodicity results are lower than those obtained by Truong and Nguyen for all Reynolds numbers investigated and this may be attributed to the current investigation ensuring fully developed Tesla valve inlet flow (via

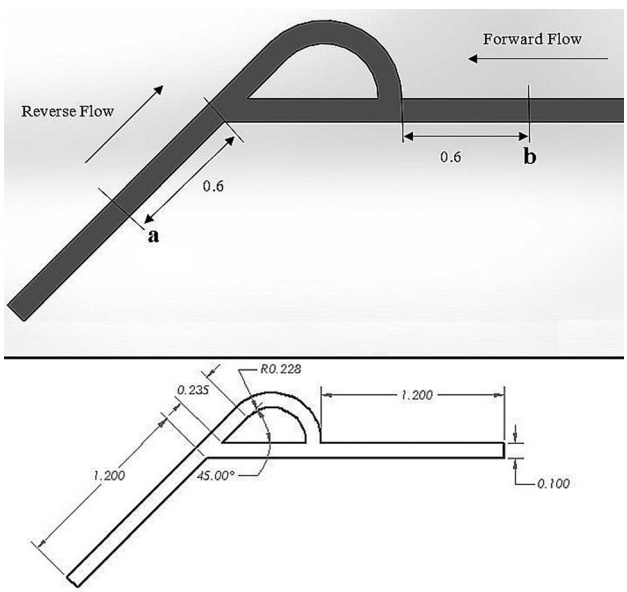

Fig. 3 T45-R Tesla valve (depth = 0.1 mm) with extended entrance/exit lengths and pressure measurement locations (*a*) and (*b*). All units in millimeters.

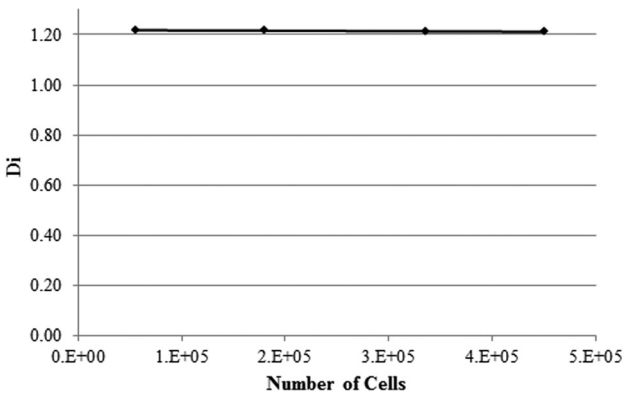

Fig. 4 Diodicity versus number of cells for extended T45-R Tesla valve at Re = 300

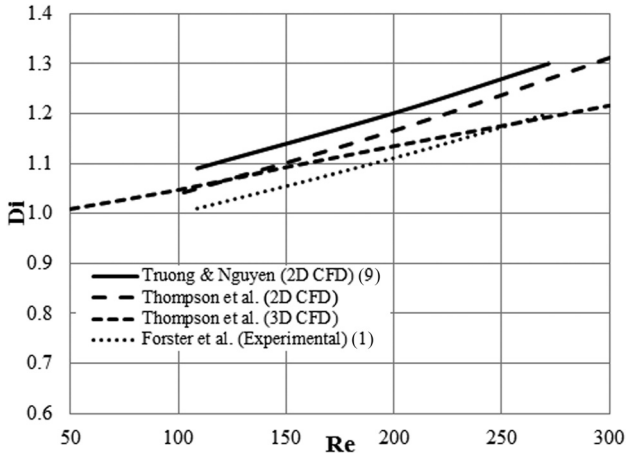

Fig. 5 Diodicity versus Reynolds number for T45-R Tesla valve determined using CFD simulations and experimental data

extended entrance/exit lengths) and imposing a more refined mesh. Since the current 3D CFD results agree within 4% (maximum relative error) of the Forster et al. experimental results, the current solution methodology is assumed to be sufficiently validated for investigation of the effects of multistage valve geometries. It is confirmed that 3D CFD simulations provide for more accurate predictions of Tesla valve diodicity compared to 2D CFD simulations that overpredict the experimental measurements and appear to diverge at higher Reynolds numbers where secondary flows are more pronounced.

The T45-R Tesla valve, although used to confirm a valid, mesh-independent CFD approach, is not an optimally designed Tesla valve [11]. Therefore, in construction of the MSTV, an optimally shaped (GMF) Tesla valve [11] was used to serve as the individual building block. The MSTVs possessed a low-angled configuration (i.e., similar to Reed [13]) with $\theta \cong 48$ deg and each GMF Tesla valve had a square cross section with width of 1 mm. The GMF Tesla valve, with marked points for the static pressure measurements (a) and (b)—which are also the original entrance and exit lengths [11]—is shown in Fig. 6. Again, the entrance and exit lengths were extended to provide for fully developed flow conditions prior to fluid entering the original entrance/exit. Like the T45-R Tesla valve, local transitional flows were observed to occur for Re $\gtrsim$ 300. As a result, low Reynolds numbers were utilized to ensure that complete laminar conditions existed along the entire GMF Tesla valve and only laminar solving methods were used. Mesh resolution levels for the GMF Tesla valves were consistent with those obtained from the mesh independent study on the similar T45-R valves. A planar perspective of the employed meshing-scheme is shown in Fig. 7 for a two-staged MSTV (with GMF-styled Tesla valves).

GMF Tesla valves were connected in series to form various MSTVs. The MSTV parameters varied were: the number of Tesla valve stages (N) and the valve-to-valve distance (l). The valve-to-valve distance, which is the distance between adjacent Tesla valves, was nondimensionalized using the main channel hydraulic diameter

$$G = \frac{l}{D_H} \tag{4}$$

The dimensionless valve-to-valve distance G was varied from a compact (small clearance) distance, $G = 0.675$ ($l = 0.675$ mm), to a relative large distance, $G = 3.375$.

Similar to finding the diodicity of a single GMF Tesla valve, the MSTV diodicity was found by taking the mass-averaged, static pressure measurement at 2.1 mm upstream of the first Tesla valve (with respect to forward direction) and 2.94 mm downstream of the last Tesla valve (with respect to the forward

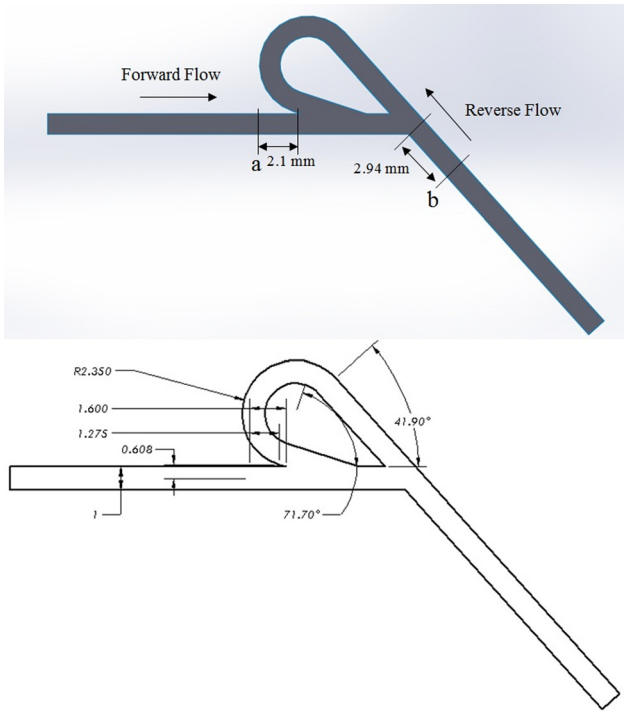

Fig. 6 GMF Tesla valve (depth = 1 mm) with extended entrance/exit lengths and pressure measurement locations (*a*) and (*b*). All units in millimeters.

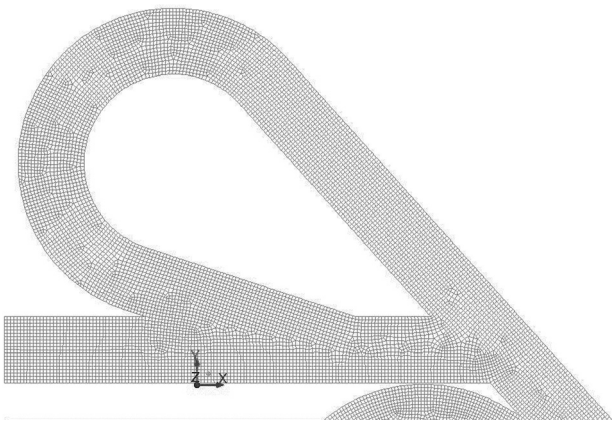

Fig. 7 Mesh utilized for the MSTV ($N = 2$)

direction) or vice versa for reverse flow. A 3D rendering of the MSTV with $N = 8$ and $G = 0.675$ is shown in Fig. 8(*a*). Two MSTVs with $N = 4$, each with a different valve-to-valve distance, are shown in Figs. 8(*b*) and 8(*c*). The primary cases investigated are summarized in Table 1.

Results and Discussion

Diodicity. The effect of varying the number of Tesla valves and Reynolds number (for minimum G) on the MSTV diodicity is shown in Fig. 9. It is observed that the MSTV diodicity, like the diodicity of a single Tesla valve, increases nonlinearly with Reynolds number. For a given Reynolds number, the MSTV diodicity increases with higher valve number and this becomes more pronounced at higher Reynolds numbers. The percent enhancement in diodicity, defined as the percentage increase in diodicity relative to a single GMF Tesla valve, for the low-angled MSTV ($\theta \cong 48$ deg, with GMF Tesla valves) is illustrated in Fig. 10.

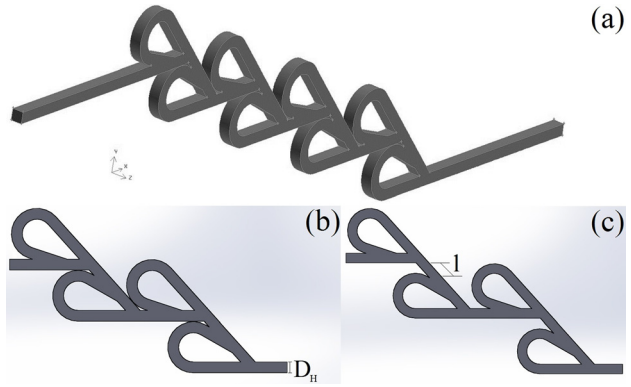

Fig. 8 Multistaged Tesla valve with (*a*) $N = 8$ and $G = 0.675$; and MSTV with $N = 4$: (*b*) $G = 0.675$ and (*c*) $G = 2.025$

Table 1 Parameter values used for the MSTV numerical investigation

Parameter	Values
Re	25, 50, 75, 100, 125, 150, 175, 200
N	1, 2, 4, 6, 8, 10, 20
G	0.675, 0.84, 1.35, 2.025, 3.375

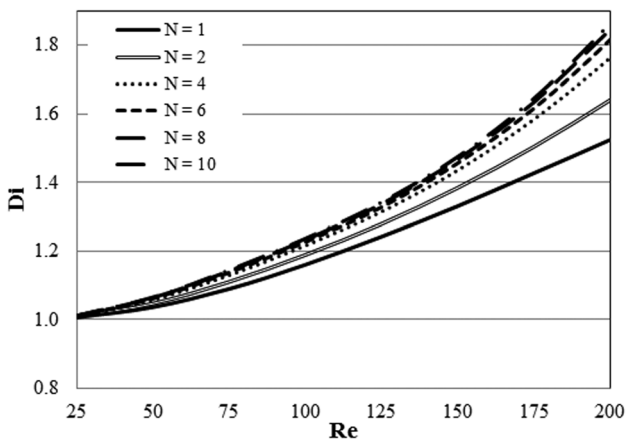

Fig. 9 Diodicity versus Reynolds number for various number of Tesla valve stages ($G = 0.675$)

From the figure it may be observed that for $\mathrm{Re} = 200$, increasing the valve number from $N = 1$ to $N = 10$ increases the diodicity by almost 25% to values near $Di \sim 1.9$. It may also be seen that the percentage enhancement in diodicity depends heavily on Reynolds number, with three distinct regimes being observed. In the ultra-low Reynolds number regime ($\mathrm{Re} \lesssim 75$) the percent enhancement is approximately linear regardless of valve number. For $75 \lesssim \mathrm{Re} \lesssim 125$, the percent enhancement still increases linearly with Reynolds number but with a lower slope. Finally, for $\mathrm{Re} \gtrsim 125$, the percent enhancement increases much more rapidly and nonlinearly with Reynolds number. These results indicate that MSTVs may be more beneficial for larger channel diameters and/or fast-moving fluids.

The static pressure differences across various-staged MSTVs and Reynolds numbers for forward and reverse flow directions are shown in Figs. 11(*a*) and 11(*b*), respectively. The forward pressure difference is observed to be always less than the reverse pressure difference, confirming the fluidic diode effect of the MSTV. The forward pressure difference is also more linear for the range of Reynolds numbers investigated. The nonlinearities in the reverse flow pressure difference are attributed to the minor

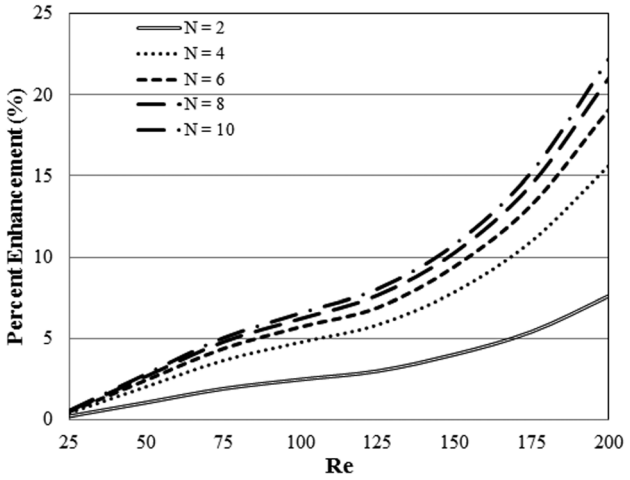

Fig. 10 Percentage enhancement versus Reynolds number for various number of Tesla valve stages ($G = 0.675$)

pressure losses such as flow bifurcation and impingement at each stage. During forward flow, the arcs of the Tesla valves are almost completely bypassed, allowing for a nearly linear pressure profile that is governed primarily by major, viscous flow losses similar to simple duct flow. The forward and reverse pressure difference increases as the number of Tesla valve stages increases for a given Reynolds number.

The effect of dimensionless valve-to-valve distance on the MSTV diodicity for various Reynolds numbers is shown in Fig. 12. It is apparent that the MSTV diodicity is sensitive to the valve-to-valve distance and this dependence becomes more pronounced as the Reynolds number increases. For $\mathrm{Re} \geq 100$, minimization of the valve-to-valve distance will significantly increase the MSTV diodicity. For very low Reynolds numbers ($\mathrm{Re} = 50$), the MSTV diodicity is nearly independent of valve-to-valve distance. Figure 12 also demonstrates that the MSTV diodicity approaches the diodicity of a single Tesla valve as $G \rightarrow \infty$, as expected. Interestingly, however, for $\mathrm{Re} = 200$ and $G = 3.375$, the MSTV ($N = 6$) diodicity is actually lower than for a single Tesla valve ($Di \lesssim 1.52$).

It may be seen in Fig. 13 that as the number of Tesla valves increases (for a given Reynolds number); the valve-to-valve distance may be increased with little detriment to the MSTV diodicity. For fully laminar Tesla valve flow ($\mathrm{Re} \lesssim 200$), the MSTV diodicity becomes nearly independent of the number of Tesla valves utilized for $G \geq 2$. However, based on Figs. 12 and 13, this "critical" dimensionless valve-to-valve distance increases slightly with higher Reynolds numbers.

The effect of the number of Tesla valves on the MSTV diodicity for various Reynolds numbers is shown in Fig. 14. It may be seen from the figure that, for a given Reynolds number, a critical number of Tesla valves exists, beyond which increasing N provides little further increase in MSTV diodicity. This critical valve number increases as the Reynolds number increases. Therefore, more Tesla valves are required for higher Reynolds numbers in order to maximize diodicity. For example, at $\mathrm{Re} = 50$, two tightly packed (i.e., $G = 0.675$) Tesla valves are sufficient for near maximization of MSTV diodicity. However, for $\mathrm{Re} = 200$, approximately ten tightly packed Tesla valves are required for maximizing MSTV diodicity. For all Reynolds numbers investigated, increasing the valve number from one to two can provide for significant enhancement in diodicity, consistent with the results reported by Mohammadzadeh et al. [15].

Multivariable data fitting was performed numerically with the assistance of MATLAB® (v. 7.14) and *Mathematica*® (v. 9) in order to determine a correlation for MSTV diodicity based on the dimensionless parameters investigated. First, for $G = 0.675$, a

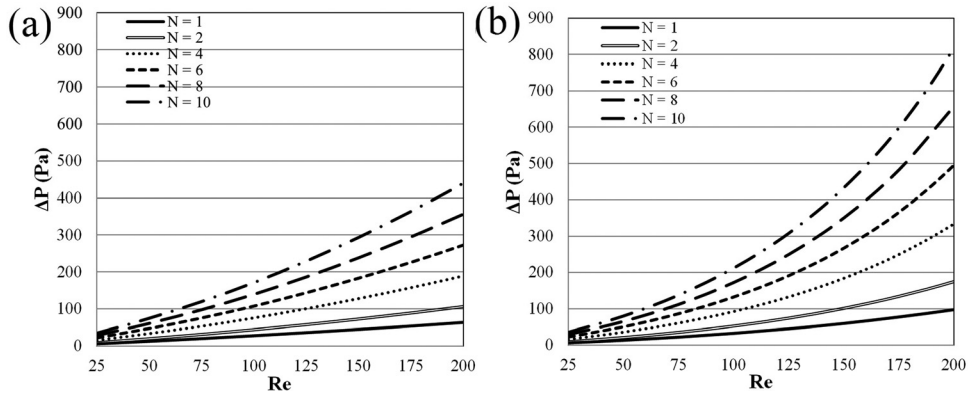

Fig. 11 Static pressure difference versus Reynolds number various number of Tesla valve stages ($G = 0.675$) during (*a*) forward flow and (*b*) reverse flow.

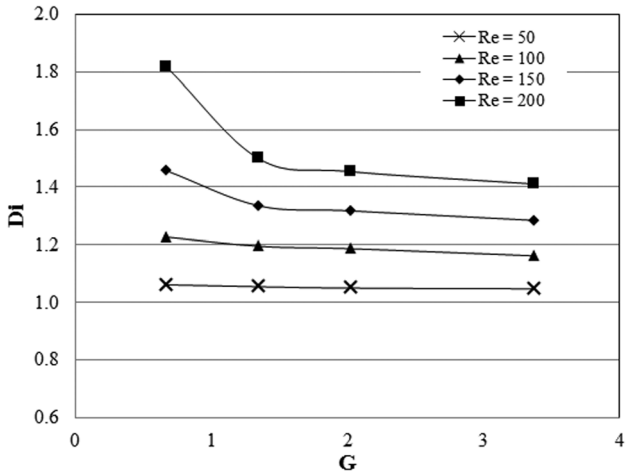

Fig. 12 Diodicity versus nondimensional valve-to-valve distance for various Reynolds numbers ($N = 6$).

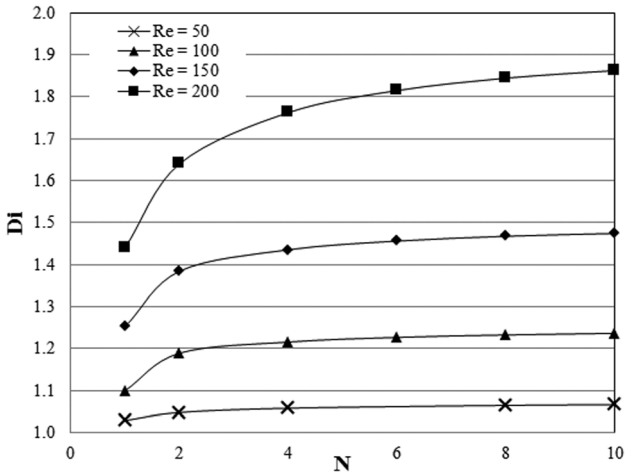

Fig. 14 Diodicity versus number of Tesla valves (N) for various Reynolds numbers ($G = 0.675$)

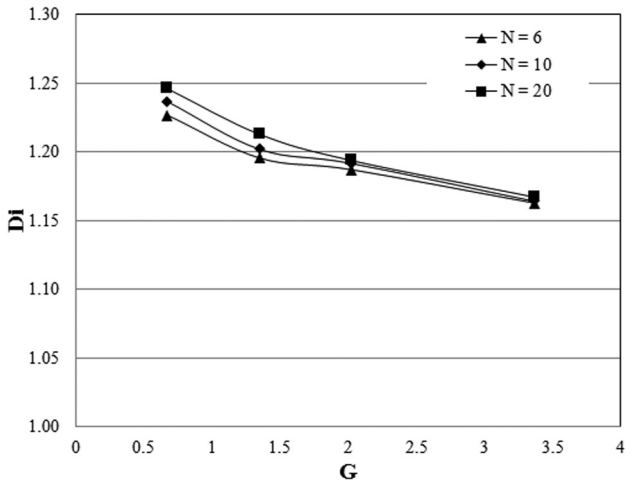

Fig. 13 Diodicity versus nondimensional valve-to-valve distance for various number of Tesla valves with Re = 100

custom function was constructed as to minimize the coefficient of determination (R^2) for predicting the dependent variable Di for the independent variables N and Re. It was found that diodicity is well predicted ($R^2 \cong 0.9931$) using

$$Di \cong 1 + 4.78\times10^{-5}\left(N^{0.16}\mathrm{Re}^{1.72}\right) \tag{5}$$

Considering the entire parameter space, it was found that the general functional form may be expressed as

$$Di \approx a + b\left(N^{c}G^{d}\mathrm{Re}^{e}\right) \tag{6}$$

where $a \approx 1$, $b \sim 10^{-6}$, $c \sim 10^{-1}$, d $\sim -10^{-1}$, and $e \sim 1$. Based on this functional form, a correlation was found to predict Di based on all investigated independent variables (with ranges summarized in Table 1)

$$Di \approx 0.92 + 2.67\times10^{-5}\left(N^{0.11}G^{-0.39}\mathrm{Re}^{1.87}\right) \tag{7}$$

The maximum of the absolute value of residuals (infinity norm) from Eq. (7) was minimized to be approximately 0.12. When comparing the diodicity predicted from Eq. (7) with that of numerically predicted diodicity, the maximum relative percentage error did not exceed 11%. The data-fitting procedure clearly indicates that there is a power-law dependence of the diodicity on the number of Tesla valves, valve-to-valve distance, and Reynolds number.

Static Pressure and Velocity. Contours of the static pressure (along the half-depth plane) in the forward and reverse flow directions for the MSTV with $N = 2$ and $G = 0.84$ for $\mathrm{Re} = 200$ are shown in Figs. 15(*a*) and 15(*b*), respectively. It is apparent that the two-staged MSTV provides for a higher static pressure

difference (~ 323 Pa) in the reverse flow direction than in the forward flow direction (~ 275 Pa). In both flow directions, the major pressure loss due to viscous flow is observed in the channel segments prior to the Tesla valves. In the forward flow direction, minor pressure loss is primarily between Tesla valves and this is attributed to the bended structure disturbing the flow. In the reverse flow direction, minor pressure loss due to flow bifurcation and impingement is observed at the inlet and outlet of each Tesla valve stage, respectively.

These minor losses are more clearly apparent when plotting the centerline, static pressure along the two-staged MSTV distance for forward and reverse flow scenarios (with Re = 200, $G = 0.84$) as shown in Figs. 16 and 17, respectively. As shown in Fig. 16, this centerline is along the half-depth plane and does not include the arcs of the Tesla valve flow paths. For the forward flow case, the pressure losses are nonnegligible in the vicinity of each Tesla valve. Although the GMF Tesla valve is designed to minimize the amount of forward flowing fluid entering the arc, during low Reynolds number flow a small amount does enter and this leads to pressure recovery due to self impingement at the Tesla valve outlets. This is observed around 2–3 mm and 8–9 mm along the MSTV centerline length for the first and second Tesla valve, respectively. Note that the intervalve turns provide for a minor pressure loss that may become significant for MSTVs with higher intervalve angles. Pressure recovery from self-impingement aids in reducing the severity of the intervalve pressure loss.

For reverse flow, the pressure losses in the vicinity of each Tesla valve are significantly higher, as shown in Fig. 17. There is still pressure recovery, but it is more acute and occurs at the Tesla valve inlets due to combined flow bifurcation and circulation. In between the valve inlet and valve outlet, the static pressure is nearly constant due to two-dimensional flow effects; however, at locations near the valve outlet a significant pressure loss occurs due to the jet impingement and recirculation effects. The pressure loss due to impingement, during reverse flow through the two-staged MSTV, accounts for nearly 75% of the total pressure loss and is the primary mechanism for the fluidic diode effect. Note that the second-stage pressure loss is similar in magnitude to the first-stage pressure loss. Minor loss due to the bent intervalve channel structure is not significant in the reverse flow case due to the employed MSTV design.

Contours of the velocity magnitude during reverse flow through an MSTV with $N = 10$ and $G = 0.84$ for Re = 25 and Re = 200 are shown in Figs. 18 and 19, respectively. During reverse flow, high velocities exist between adjacent valves and low velocities exist in the Tesla valve outlet region where the jet impingement occurs. Also, during reverse flow, the maximum velocity is generally higher due to jetting effects in the vicinity of the recirculation region. The flow bifurcation and impingement during reverse flow are clearly visible, as well. During forward flow, the velocity is more uniform with near-zero velocity magnitude in the arc of each Tesla valve structure. Figures 18 and 19 also demonstrate the apparent symmetry in the velocity field throughout the entire MSTV, with the velocity magnitude distribution being similar for all Tesla valves. Note that; as a result of the extended entrance lengths, the flow is clearly fully developed prior to entering the MSTV either in the forward or reverse flow direction.

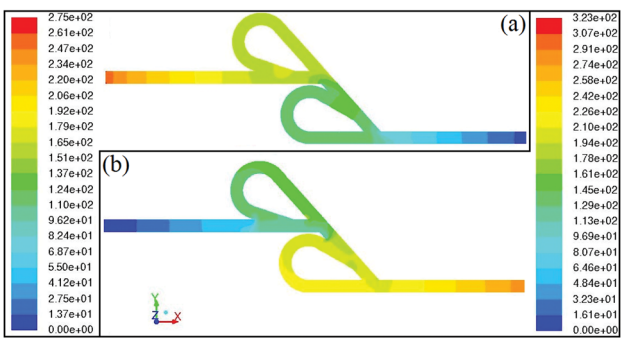

Fig. 15 Contours of static pressure (in Pa) in MSTV ($N = 2$, $G = 0.84$) for Re = 200 (on XY plane for Z = 0.5 mm) for (*a*) forward and (*b*) reverse flow

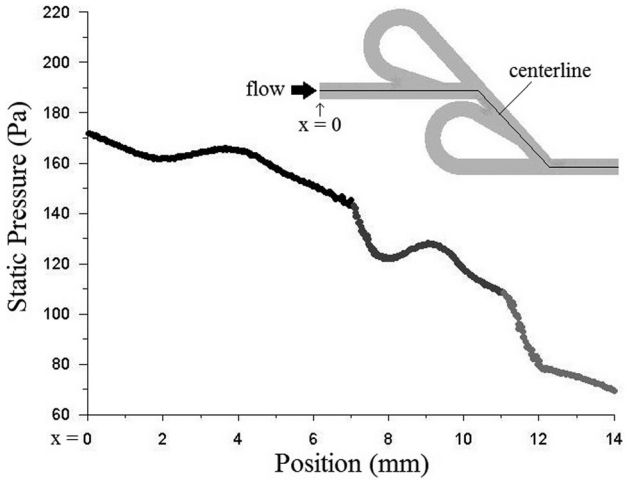

Fig. 16 Centerline static pressure versus position along a two-staged MSTV for forward flow with Re = 200, $G = 0.84$

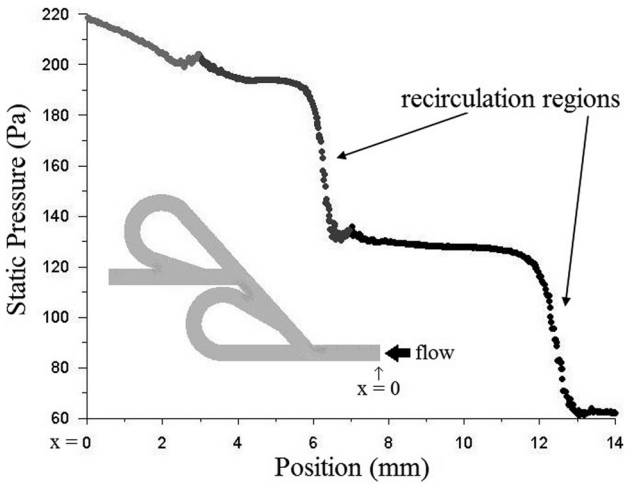

Fig. 17 Centerline static pressure versus position along a two-staged MSTV for reverse flow with Re = 200, $G = 0.84$

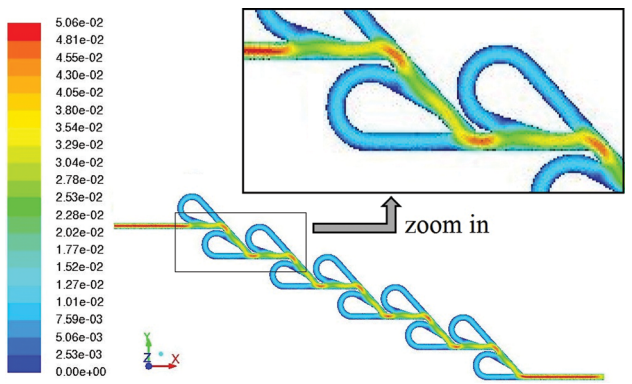

Fig. 18 Velocity magnitude (in m/s) for reverse flow in MSTV ($N = 10$, $G = 0.84$) for Re = 25 (on XY plane for Z = 0.5 mm)

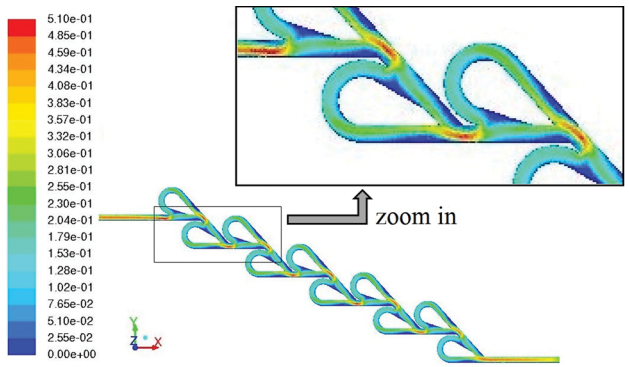

Fig. 19 Velocity magnitude (in m/s) for reverse flow in MSTV ($N = 10$, $G = 0.84$) for Re = 200 (on XY plane for Z = 0.5 mm)

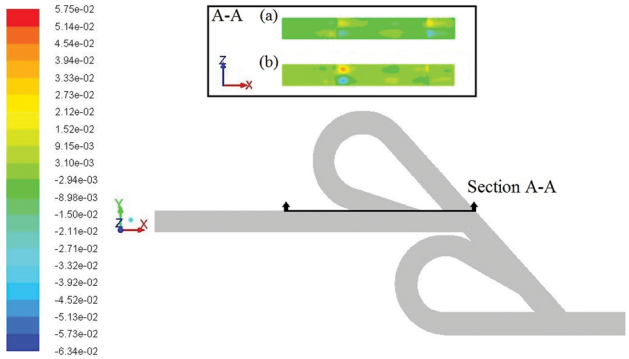

Fig. 20 Z-component of velocity (in m/s) for (*a*) forward flow and (*b*) reverse flow in MSTV ($N = 2$, $G = 0.84$) for Re = 200 (on XZ plane for Y = 0.49 mm)

The 3D characteristics during forward and reverse flow were investigated for a two-staged MSTV ($N = 2$) with $G = 0.84$ and $\mathrm{Re} = 25$ and $\mathrm{Re} = 200$ as shown in Figs. 20(*a*) and 20*b*, respectively. The magnitude of the z-velocity in the X-Z plane aligned along and near the valve-side wall of the downstream valve was investigated. It may be seen that a Z-component of velocity indicative of secondary flow does exist for both Reynolds numbers and is located in the vicinity of the Tesla valve outlet. The magnitude of the Z-component of velocity is at least an order of magnitude less than the X and Y components and increases with Reynolds number. However, the Z-velocity magnitude is nearly 15% of the X-velocity magnitude for $\mathrm{Re} = 200$, and this is significant. Note that, near the Tesla valve outlet, the top half of the MSTV channel has a positive Z-velocity component, while the bottom half has a negative Z-component. This indicates that there is out-of-plane circulation near the corner of the Tesla valve outlet. This is a result of three-dimensional flow turning, leading to complex secondary flow features within the shear layer. The details of the secondary flow affect the reverse flow pressure drop and help explain the need for 3D CFD to accurately simulate the Tesla valve fluid dynamics.

Conclusions

Using 3D CFD, the effectiveness of multistaged Tesla valves (MSTVs), created by arranging multiple Tesla valves in series, was quantified in terms of diodicity and investigated for low Reynolds numbers and various valve-to-valve distances. Each MSTV consisted of identical, preoptimized Tesla valves and possessed an intervalve angle of approximately $\theta = 48$ deg (i.e., low-angled MSTV). The implemented CFD ensured fully laminar flow conditions throughout the entire MSTV and fully developed flow prior to first-stage MSTV inlet. The major conclusions are as follow:

(1) Utilizing the Tesla valves in series provides for a marked increase in diodicity. Depending on flow/design, the MSTV can provide up to $Di \sim 1.9$ for $\mathrm{Re} = 200$, versus $Di \sim 1.5$ for a single-stage valve ($\sim 23\%$ enhancement).
(2) The MSTV diodicity increases nonlinearly with Reynolds number. For a given Reynolds number, the MSTV diodicity increases with higher valve number. There is a power-law dependence of the diodicity on the number of Tesla valves, valve-to-valve distance, and Reynolds number.
(3) Minimizing the valve-to-valve distance yields a higher MSTV diodicity, with the increase becoming greater as the Reynolds number increases.
(4) For a given Reynolds number, increasing the valve-to-valve distance decreases the MSTV diodicity until it eventually becomes equal to (or in some cases slightly less than) the single Tesla valve diodicity.
(5) For low Reynolds number ($\mathrm{Re} \sim 50$), the number of Tesla valves, as well as the valve-to-valve distance, has little effect on MSTV diodicity.
(6) For fully laminar Tesla valve flow ($\mathrm{Re} \lesssim 200$), the MSTV diodicity becomes nearly independent of the number of Tesla valves utilized for nondimensional valve-to-valve distances, $G \geq 2$.
(7) As the Reynolds number is increased, more Tesla valves are required to maximize the MSTV diodicity. For a given Reynolds number, the MSTV diodicity is asymptotic with respect to the number of Tesla valves used.
(8) The primary mechanism responsible for flow resistance in the reverse flow direction through a MSTV is jet impingement at the individual Tesla valve outlets.

The current investigation has also demonstrated that using 3D CFD, as opposed to 2D CFD, more accurately predicts the diodicity of a Tesla valve. The velocity vector field has three-dimensional secondary flow characteristics near the vicinity of the Tesla valve outlets. The importance of ensuring fully developed flow prior to the Tesla valve inlet and fully laminar conditions throughout the entire Tesla valve structure have also been determined. For example, although the Reynolds number may be laminar at the Tesla valve inlet (i.e., $\mathrm{Re} < 2300$), local transitional and turbulent flows occur at or around the Tesla valve junctions, and this influences the selected CFD solver accuracy and convergence. Based on the investigated Tesla valves, transitional flows were found to occur around $\mathrm{Re} \approx 300$.

Nomenclature

D = diameter, m
Di = diodicity
G = nondimensional valve-to-valve distance
l = valve-to-valve distance, m
N = number of Tesla valves (stages)
P = static pressure, Pa
R^2 = coefficient of determination
Re = Reynolds number
u = speed or velocity vector, m/s
x = spatial coordinate, m

Greek Symbols

μ = dynamic viscosity, Pa·s
ν = kinematic viscosity, m^2/s
ρ = density, kg/m^3
θ = intervalve angle

Subscripts

f = forward
H = hydraulic

i = inlet
i, j = Cartesian indices
r = reverse

References

[1] Forster, F. K., Bardell, R. L., Afromowitz, M. A., Sharma, N. R., and Blanchard, A., 1995, "Design, Fabrication and Testing of Fixed-Valve Micro-Pumps," Proc. ASME Fluid Eng. Div., **234**, pp. 39–44.

[2] Stemme, E., and Stemme, G., 1993, "A Valveless Diffuser Nozzle-Based Fluid Pump," Sensors Actuators A Phys., **39**, pp. 159–167.

[3] Gerlach, T., 1998, "Microdiffusers as Dynamic Passive Valves for Micropump Applications," Sensors Actuators A Phys., **69**, pp. 181–191.

[4] Tasi, C. H., Lin, C. H., Fu, L. M., and Chen, H. C., 2012, "High-Performance Microfluidic Rectifier Based on Sudden Expansion Channel With Embedded Block Structure," Biomicrofluidics **6**, pp. 24108–241089.

[5] Fadl, A., Zhang, Z., Geller, S., Tolke, J., Krafczyk, M., and Meyer, D., 2009, "The Effect of the Microfluidic Diodicity on the Efficiency of Valve-Less Rectification Micropumps Using Lattice Boltzmann Method," Microsyst. Tech., **15**, pp. 1379–1387.

[6] Tesla, N., 1920, –"Valvular Conduit," U.S. Patent NO. 1,329,559.

[7] Bardell, R. L., 20001, "The Diodicity Mechanism of Tesla-Type No-Moving-Parts Valves," Ph.D. dissertation, University of Washington, Seattle, WA.

[8] Paul, F. W., 1969, "Fluid Mechanics of the Momentum Flueric Diode," IFAC Symposium on Fluidics, Royal Aeronautical Society, Paper A1, pp. 1–15.

[9] Truong, T. Q., and Nguyen, N. T., 2003, "Simulation and Optimization of Tesla Valves," 2003 Nanotech - Nanotechnology Conference and Trade Show, San Francisco, CA, pp. 178–181.

[10] Zhang, S., Winoto, S. H., and Low, H. T., 2007, "Performance simulations of Tesla Microfluidic Valves," Proceedings of the International Conference on Integration and Commercialization of Micro and Nanosystems, Sanya, Hainan, China, Paper No. MNC2007-21107 A., pp. 15–19.

[11] Gamboa, A. R., Morris, C. J., and Forster, F. K., 2005, "Improvements in Fixed-Valve Micropump Performance Through Shape Optimization of Valves," ASME J. Fluid Eng., **127**, pp. 339–346.

[12] Thompson, S. M., Ma, H. B., and Wilson, C. A., 2011, "Investigation of a Flat-Plate Oscillating Heat Pipe With Tesla-Type Check Valves," Exp. Therm. Fluid Sci., **35**, pp. 1265–1273.

[13] Reed, J. L., 1993, –"Fluidic Rectifier," U.S. Patent No. 5,265,636.

[14] Afromowitz, M. A., Bardell, R. L., Blanchard, A. P., Forster, F. K., and Sharma, N. R., 1999, –"Micropumps With Fixed Valves," U.S. Patent No. 5,876,187.

[15] Mohammadzadeh, K., Kolahdouz, M. E., Shirani, E., and Shafii, M. B., 2012, "Numerical Investigation on the Effect of the Size and Number of Stages on the Tesla Microvalve Efficiency," J. Mech., **29**, pp. 527–534.

[16] Patankar, S. V.,1980, *Numerical Heat Transfer and Fluid Flow*. Hemisphere, Washington, DC.

[17] Rhie, C. M., and Chow, W. L., 1983, "Numerical Study of the Turbulent Flow Past an Airfoil With Trailing Edge Separation," AIAA J., **21**, pp. 1525–1532.

[18] Barth, T. J., and Jesperson, D., 1989, "The Design and Application of Upwind Schemes on Unstructured Meshes," Proceedings of the 27th AIAA Aerospace Sciences Meeting, Reno, NV, Technical Report AIAA-89-0366.